Effect of Vacuum System Base Pressure on Corrosion Resistance of Sputtered Al Thin Films

G. S. Frankel,[a,*,z] X.-B. Chen,[b] R. K. Gupta,[b] S. Kandasamy,[c] and N. Birbilis[b,]**

[a]*Fontana Corrosion Center, The Ohio State University, Columbus, Ohio 43210, USA*
[b]*Department of Materials Engineering, Monash University, Clayton, Victoria 3216, Australia*
[c]*Melbourne Centre for Nanofabrication, Clayton, Victoria 3216, Australia*

Pure aluminum (Al) thin films were sputter deposited under conditions of variable base pressure of the deposition tool. The purpose of the study was to identify if the base pressure had a key influence on the electrochemical properties, namely corrosion resistance, of the Al deposits. The corrosion resistance was found to increase with increasingly high base pressure (i.e. lower quality vacuum). Potentiodynamic polarization experiments, pit growth studies, TEM and XPS were employed. From the results is posited that improved corrosion resistance is due to the presence of oxygen (O) being incorporated into the films during deposition resulting an O-containing (i.e. Al-O) alloy. This effect is important to identify because of the many reports in the literature of high pitting potentials for Al thin films, from studies with widely varying base pressure. Vacuum system base pressure was found to have a large effect on the corrosion resistance. A maximum base pressure in the low 10^{-7} Torr range is recommended to minimize oxygen uptake into the film.
 [DOI: 10.1149/2.056404jes]

Manuscript submitted January 6, 2014; revised manuscript received January 31, 2014. Published February 11, 2014. This was Paper 1812 from the San Francisco, California, Meeting of the Society, October 27–November 1, 2013.

Corrosion of thin film metal samples deposited by sputter deposition or evaporation has attracted considerable attention because of the technological applications of thin films in the electronics industry. From a research perspective, thin films also provide unique opportunities for studying fundamental aspects of the pitting phenomenon and also for the investigation of non-equilibrium alloy compositions. Many papers report an increased corrosion resistance of thin films relative to bulk alloy counterparts, often expressed as an increase in the pitting potential, E_{pit}.[1–11] Other researchers have found E_{pit} for thin films to be similar to bulk alloys of a similar composition.[12,13]

Several different reasons for the improved corrosion resistance of thin films have been offered. Liu and coworkers proposed that the increase in pitting resistance of Ni-based alloy thin films resulted from the nanocrystalline microstructure of the films.[4–7] Regarding the role of grain size on corrosion resistance, both increases and decreases in corrosion resistance with decreasing grain size have been reported,[14] with the phenomenon being closely related to test environment.[15] Because a fine grain structure has more reactive sites with respect to oxide formation and film ion conduction, the relative rates of reaction in a given environment might be altered. However, it is unlikely that grain size variation alone can explain the very noble values of E_{pit} that have been reported for some pure metal thin film samples.

Factors other than grain size have been reported to result in ennobled E_{pit} values in thin film samples.[16] For alloys that pit at specific sites in a heterogeneous microstructure, such as MnS particles in stainless steel, improved homogeneity achieved by sputtering can certainly improve the corrosion performance. This chemical effect, as opposed to a structural effect, has been invoked by some as an important factor when evaluating sputtered stainless steel or Fe-Cr alloys.[1,9]

Inturi and Szklarska-Smialowska investigated a number of different sputtered thin film materials. In one study, they suggested that the corrosion of Fe, Fe-Cr, Fe-W, and Fe-Ta was controlled by a fine distribution of oxide particles in the metallic film, and that the oxygen originated from the sputter targets.[2] In another study, they attributed improvement in thin film Al to the same phenomenon, even though no oxide particles were observed,[3] They also suggested in a subsequent study that the higher E_{pit} observed for sputtered SS304 resulted from a combination of the high homogeneity and the nanocrystalline microstructure.[1] In a separate publication, these authors suggested that the E_{pit} of sputtered Al and Al binary alloys was controlled by the solubility of alloying element oxides in HCl solutions representative of local pit environments.[17] Frankel et al. explained how the dissolution kinetics of pits were greatly ennobled in similar sputtered Al binary alloys, which resulted in much higher potentials being required to provide the pit current densities needed to maintain the critical pit environment to prevent repassivation.[18] However, these sputtered Al alloys cannot be compared to the performance of bulk alloys because of the limited solubility of most of the alloying elements under equilibrium conditions achieved using standard casting of bulk samples. In this case, the improved corrosion properties can be attributed to the homogeneous microstructure containing supersaturated concentrations of alloying elements for the sputter-deposited samples, i.e. a chemical effect.

An important factor when comparing the performance of thin film and bulk samples is the quality of the vacuum in the deposition chamber, as reflected by the system base pressure. Prior to deposition, a sputter-deposition or evaporation tool is pumped down to some pressure, the level of which depends on the pumping time and the quality of the vacuum and pumping systems. The pressure increases during deposition, but the level of residual contaminant gas in the system will depend on the base pressure prior to deposition. Some authors have included the base pressure prior to deposition in their experimental details[1–7,13,19] and some have not.[8,10,11,20,21] It is interesting that some of the reports of improved corrosion resistance of thin films used deposition systems with relatively poor base pressures. For example, Inturi and Szlarska-Smialowska used a system with a base pressure of about 1×10^{-6} Torr[1–3,17] and Liu and coworkers used a system with a base pressure of only 4×10^{-5} Torr.[4–7] In contrast, the reports of thin film material with corrosion properties similar to those of bulk materials used deposition systems with base pressure of 3×10^{-7} Torr, or less.[12,13]

A recent paper showed how the corrosion and electrical properties of AlO_xN_y thin films changed as oxygen and nitrogen were added.[22] A pure Al thin film with very low O content exhibited pitting at a potential similar to that of pure Al whereas films of varying O and N content exhibited no pitting corrosion at all, even after polarization to high potentials.

The purpose of the present work is to make a systematic study of the effect of base pressure on the pitting resistance of pure Al thin films in a chloride solution. Al thin films of 100 nm in thickness were sputter deposited with four different base pressures.

*Electrochemical Society Fellow.
**Electrochemical Society Active Member.
[z]E-mail: frankel.10@osu.edu

Experimental

Al thin films were deposited using a dual AC (40 KHz) magnetron sputter deposition tool (Intlvac). Two Al metal targets of 99.99% purity were employed. Ultra clean microscopic glass slides were used as inert substrates. Prior to the deposition process, the sputtering chamber was evacuated to different base pressures for different runs: 5.0×10^{-6}, 5.0×10^{-7}, 1.0×10^{-7} or 9.98×10^{-8} Torr. A Stanford Research System RGA100 residual gas analyzer was used to analyze the contamination present in the system base vacuum, specifically water vapor. High purity (99.999%) Ar gas at a flow rate of 20.0 sccm was introduced into the chamber, where a pressure of 1.0×10^{-3} Torr was achieved during deposition. The distance between the sample holder and the Al metal targets was 10.0 cm. At 300 W, a deposition rate of 17 nm/min was achieved. A film thickness of approximately 100 nm was deposited during each run.

Potentiodynamic polarization curves were measured using a 'flat-cell' (PAR, K0235, Princeton Applied Research) containing 300 mL of 0.1 M NaCl. The exposed sample area of 1 cm^2 defined by a Teflon o-ring was used as the working electrode, and a saturated calomel electrode (SCE) and Pt mesh were used as reference and counter electrodes, respectively. The electrolyte was exposed to air. Electrochemical experiments were performed with a BioLogic VMP-3Z potentiostat using EC-Lab 10.32 software (BioLogic) at a sweep rate of 1 mV/s after 10 min of exposure at the open circuit potential (OCP). The scans started at 10 mV below OCP. E_{pit} was taken as the value at which the current dramatically increased, which was clearly delineated in the polarization curves (as shown below). Experiments that exhibited evidence of crevice corrosion were not subsequently included in the analysis. At least 3 separate scans were performed for each data point to provide a measure of reproducibility.

Sheet resistance of the Al films sputtered at various base pressures was measured with a Jandel Model RM3 four-point probe. The test was performed five times on each sample (at different locations) and the mean value was calculated. Since the Al films had the same thickness, the sheet resistance is used here to indicate conductivity.

Thin film pit growth experiments were performed in air-exposed 0.1 M NaCl solution using procedures developed and described previously.[18,19] The thin film sample surface was viewed and recorded continuously using a video system. The sample was illuminated from above, which provided strong contrast between the black pitted region and the reflective unpitted region. The potentiostat was controlled manually in potentiostatic mode to allow for instantaneous control of the applied potential. The potential was stepped progressively upwards using steps typically 50 mV in size and 30 s in duration, As the potentiodynamically-determined E_{pit} approached, step size was decreased to 20 mV. The upward stepping continued until the current increased dramatically, which was always associated with the initiation of a pit. As has been found previously for thin film samples,[18,19] the pits penetrated the 100 nm film quickly, reached the glass substrate, and then propagated outwards. The position of the sample was adjusted such that the growing pit perimeter was always in the field of view of the video recording system. After the image of the growing pit was recorded for a short period (typically less than 10 s for high pit growth rates and greater than 30 s for slower pit growth rates), the potential was stepped downwards and the image of the growing pit was recorded at the lower potential. The potential was typically stepped by 50 mV when the applied potential was high and the pit growth was rapid. At lower potentials where the pit growth rate was slower, the magnitude of the potential step was only 10 mV to provide better resolution of the data. The experiment was stopped when the pit stopped growing at some low potential, which was considered to be the repassivation potential, E_{rp}. The pit growth kinetics were determined by analysis of the recorded images from the velocity of the thin film pit wall at a constant potential in the direction of pit growth.

Surface chemistry was analyzed by X-ray photoelectron spectroscopy (XPS) using a Thermo K-alpha spectrometer with a hemispherical analyzer. The core level XPS spectra for Al2p, O1s and C1s were recorded. The measured binding energy values were calibrated by the C1s (hydrocarbon C-C, C-H) peak at 285 eV. The photoelectrons were generated by Al-Kα (1486.6 eV) primary radiation (20 kV, 15 mA).

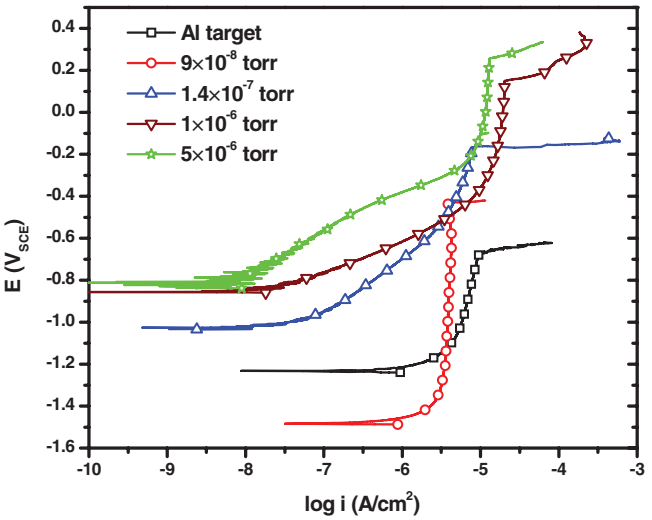

Figure 1. Potentiodynamic polarization anodic curves of Al target used for film sputtering, and Al films produced at different pressures in 0.1 M NaCl.

Transmission electron microscopy was performed on samples deposited onto silicon TEM grids containing silicon nitride membrane windows, and imaging and analysis was performed on an FEI Tecnai TF-20 operating at 200 kV.

Results and Discussion

Representative potentiodynamic polarization curves in 0.1 M NaCl for various samples are shown in Figure 1. The Al samples were spontaneously passive in this neutral chloride solution and a sharp increase in current was observed at E_{pit} as a result of the initiation and growth of pits. The scans were stopped soon after the current increase to prevent consumption of a large part of the sample. However, pits could be easily seen as through-holes in the thin film samples through which light was transmitted.

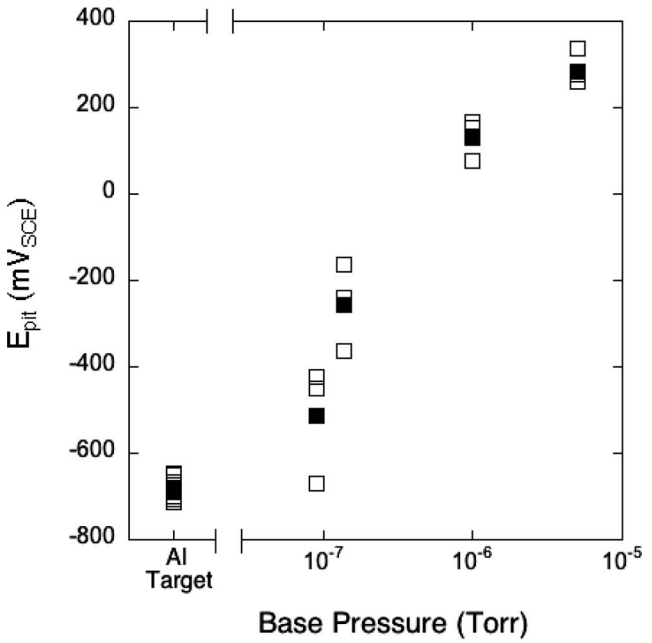

Figure 2. Summary of pitting potential data. Filled symbols represent average values and open symbols are data from all experiments performed on different samples.

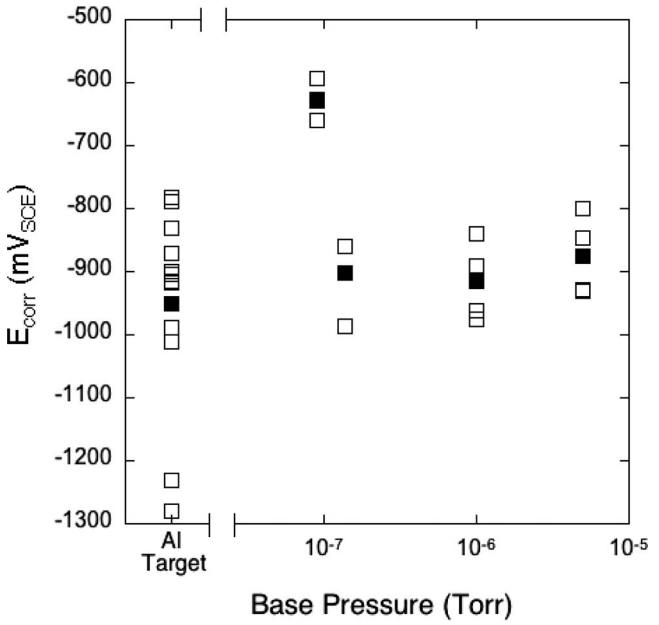

Figure 3. Summary of corrosion potential data. Filled symbols represent average values and open symbols are data from all experiments performed on different samples.

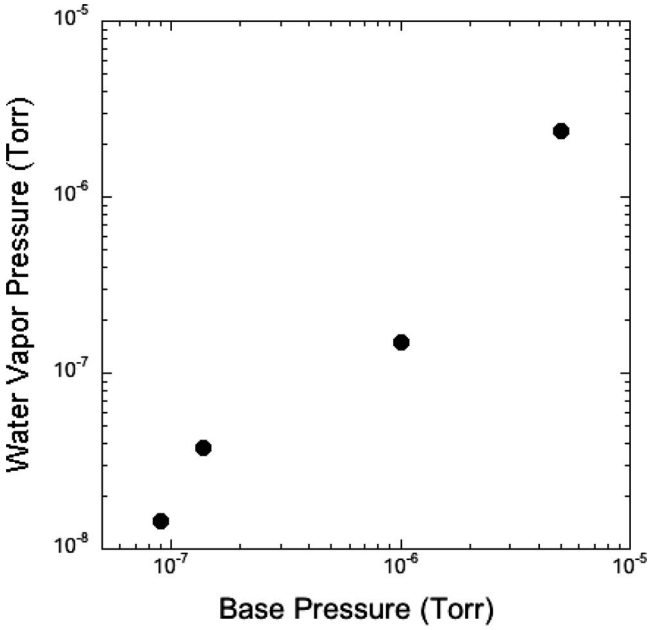

Figure 4. Water vapor pressure measured by residual gas analysis of the base vacuum as a function of base vacuum pressure.

The values of E_{pit} determined for every experiment are summarized in Figure 2 along with averages for each base pressure and for the bulk Al target used as the Al source for the thin films during deposition. The lowest E_{pit} values and the smallest extent of scatter were exhibited by the bulk Al target sample. The average value of -684 mV_{SCE} is in the range of previously reported E_{pit} for pure Al.[16] The E_{pit} values for the thin film samples were more noble than that for pure Al and increased with increasing base pressure of the vacuum system before deposition. One sample deposited with the lowest base pressure of 9×10^{-8} Torr exhibited E_{pit} in the range of the Al target, but the average was higher. The average E_{pit} of the samples deposited with highest base pressure of 5×10^{-6} Torr (the worst vacuum) was $+285$ mV_{SCE}, which is almost 1 V more noble than that observed for the target.

The corrosion potentials, E_{corr}, of all experiments and the average values are shown in Figure 3. In contrast to the tight distribution of E_{pit} values for the bulk Al target, the E_{corr} values were distributed over a wide range of potential, from -1280 to -780 mV_{SCE}. It is not unusual for passive metals to exhibit a large scatter because of the polarizibility of the passive dissolution reaction. The average E_{corr} values were generally all about the same, but the values measured for the samples deposited with a base pressure of 9×10^{-8} Torr were somewhat higher for an unknown reason.

Considering the noble values of E_{pit} and the large values of E_{pit}-E_{corr}, the data suggest that the thin film samples were extremely resistant to localized corrosion and that this resistance increased with the base pressure of the vacuum prior to film deposition. This improvement in localized corrosion resistance might be attributed to differences in the behavior of the metal, the oxide on the surface or both. Before addressing the factors that control the corrosion resistance, it is of interest to determine how the vacuum base pressure might affect the sample structure or composition.

The water vapor present in the base vacuum was assessed using residual gas analysis. Figure 4 shows that the water vapor pressure increased almost linearly with the base pressure. Both varied over a range of almost two orders of magnitude. It is also evident that water vapor is a large fraction of the total base pressure under each condition. However, the RGA was not calibrated, so the values of water vapor pressure are not precise. Water vapor is the most difficult residual to pump to ultra high vacuum level without baking or pumping the vacuum chamber for extended periods. This increase in water vapor pressure in the base vacuum seems to have altered the deposited film in a way that increases its resistance to localized corrosion.

The four-point probe measurements of sheet resistance are given in Figure 5. Compared to the bulk materials, thin films have a different sheet resistance because the low thickness of films enhances collisions of electrons and surfaces, restricts electron motion, and thus induces a higher resistance than bulk materials.[23] The sheet resistance is also influenced by a number of factors, such as rate of deposition, temperature, grain boundaries and thickness. The increase in sheet resistance with base pressure suggests that there were variations in the metallic substrate. Incorporation of impurities or different microstructures are possible differences that might affect the sheet resistance.

The incorporation of alloying elements into Al thin films has been shown to greatly improve the corrosion properties.[13,18] Using sputter deposition, it is possible to deposit films with metastable single-phase

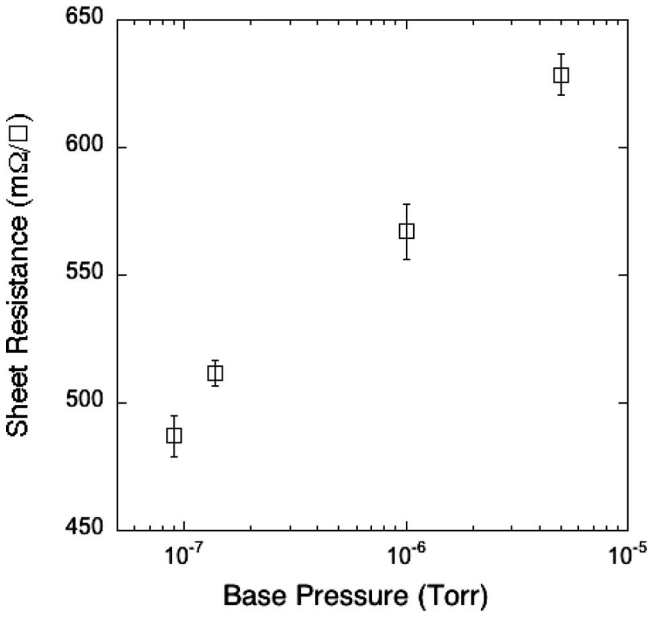

Figure 5. Forward sheet resistance measured for thin films as a function of base pressure.

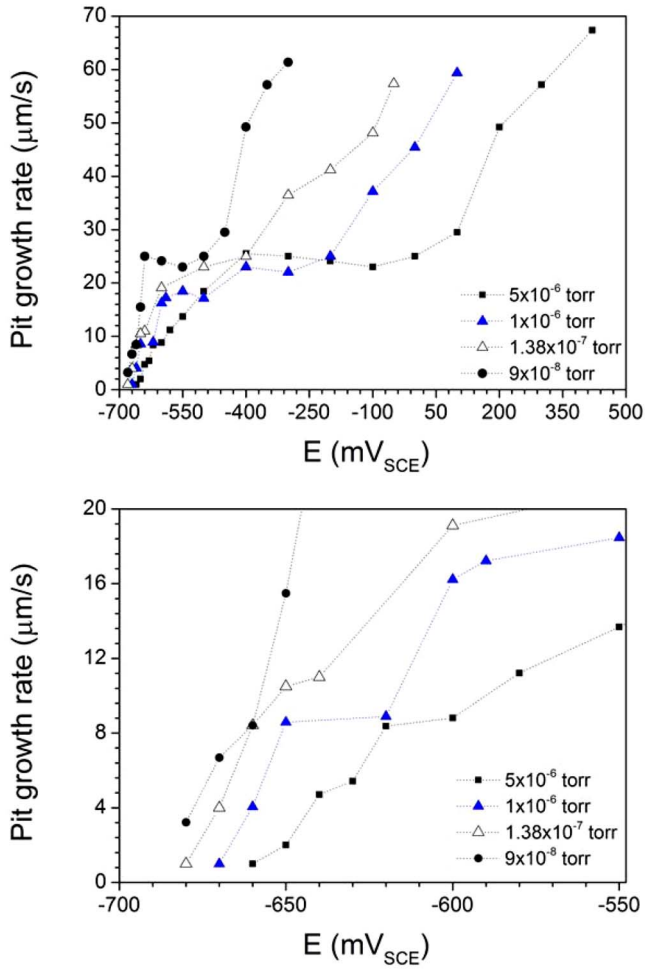

Figure 6. Thin film pit polarization curves in 0.1 M NaCl determined by image analysis of growing pits for thin films deposited with different base pressures. (a) full range of potential (b) region near repassivation expanded for clarity.

microstructures having alloy concentrations well beyond the equilibrium solubility. The determination of thin film pit growth kinetics through the analysis of images of growing pits has indicated that a large portion of the higher pitting potential of these sputtered non-equilibrium Al alloys can be attributed to the ennoblement of the dissolution reaction.[18] To test whether the pit dissolution kinetics were affected by the base pressure, thin film pit growth experiments were performed in this study. As described in the experimental section, a sample surface was observed and recorded while the potential was controlled manually. The potential was stepped upwards (to more noble values) until pit initiation was observed, and then the potential was stepped downwards until the pit repassivated. At each growth potential, the velocity of the pit wall, v, was assessed by image analysis. It is possible to determine the local pit growth current density, i, using Faraday's law:[12,18,19]

$$i = \frac{\rho n F}{M} v \qquad [1]$$

where $\rho = 2.7$ g/cm^3 is the density of Al, n = 3 eq/mol is the oxidation state of Al ions, F = 96500 C/eq is the Faraday constant, and M = 27 g/mol is the Al molecular weight, such that $i = 29$ A/cm^2 when $v = 10$ μm/s.

Figure 6 shows pit polarization curves in 0.1 M NaCl determined by image analysis of growing pits for thin films deposited with different base pressures. Figure 6a includes the full range of potentials over which pit growth was observed. The highest value for each sample is the potential at which pitting initiated during the upward stepping. It is obvious that the potential at which pitting initiated increased with increasing base pressure, which was also shown in Figure 2 for potentiodynamic testing. The values of E_{pit} were higher than those measured during potentiodynamic polarization and were not reproducible. The reason for this difference in measured breakdown potential for these experiments in which the potential was stepped upwards compared to the values measured during potentiodynamic polarization is not known. These tests were repeated a minimum of two times for each condition; the figure shows only one of each. The E_{rp} values, which are discussed below, and the currents in the lower potential region were reproducible.

All of the samples exhibited similar shaped curves, which have some differences from previously reported pit polarization curves.[12,18,19] Similar to what was reported previously, the pit current density increased with increasing potential in the low potential region, where growth is limited by ohmic and charge transfer considerations. In this region, the pit growth front was irregular with attack occurring at only a portion of the pit wall, resulting in finger-like attack. The growth rate reported in Figure 6 in this region is the rate of growth at the active fingers, not the average rate of attack along the whole pit front. At higher potentials, a limiting current density of about 22–26 μm/s (64–75 A/cm^2) was exhibited in all of the curves. In this region, the growth is limited by mass transport, and the pits were round with a uniform rate of growth in all directions. Limiting pit current densities of only 25–30 A/cm^2 were reported for thicker Al films (150 nm).[12] However, another study on NiFe thin films showed that the limiting current density for thin film pits is a sensitive function of film thickness, increasing as the film thickness decreases.[24] Therefore, the observed value of limiting current density is reasonable.

The pit polarization curves in Figure 6a exhibit a feature not seen previously for pure Al films: in the highest potential range the pit current density increased again with increasing potential. It should be recalled that the curves were collected as the potential was stepped downwards from the first breakdown observed during upward stepping. The reason for this behavior of increasing potential with potential increasing above the limiting current region is not known. It might be associated with the absence of local hydrogen evolution at the higher applied potentials.

Figure 6b shows an expanded view of the low potential region near repassivation, which occurred just below the lowest potential point for each curve. It is clear that the pit polarization curve in this region and the E_{rp} shifted to higher values of potential as the base pressure during deposition increased. This suggests that the kinetics of pit growth were ennobled because of differences in the metal film that resulted from incorporation of species in the sputtering atmosphere that was enriched in water vapor as shown in Figure 4. However, the total shift was only about 20 mV, which cannot explain the increase in E_{pit} of hundreds of mV for the same samples. In this case, the ennoblement of pit kinetics only caused part of the increase in E_{pit}.

XPS was performed to investigate differences in the surface oxide film. The samples were in the as-deposited condition with no surface pretreatment for all electrochemical tests, so the same condition was used for XPS analysis. Figure 7 shows high resolution scans of the Al 2p band for each of the samples. Two peaks are clearly observed in each spectrum, the lower energy one being associated with metallic Al and the higher energy one with oxidized Al^{3+}. The relative height of the two peaks changed with base pressure with the oxidized Al peak increasing in relative magnitude as the base pressure increased. The spectra were fitted using the commonly-adopted Shirley background subtraction and the increase in the Al^{3+}/Al^0 atomic ratio with increasing base pressure is summarized in Figure 8. The data were collected from each sample in the same way, with a 90° takeoff angle, and at the same time following deposition. The thickness of oxide layer on Al surface was also calculated using the equation exploited by Kolics et al.[25] and Strohmeier:[26]

$$d\,(\text{Å}) = 28 \ln(1.4 \frac{I_o}{I_m} + 1) \qquad [2]$$

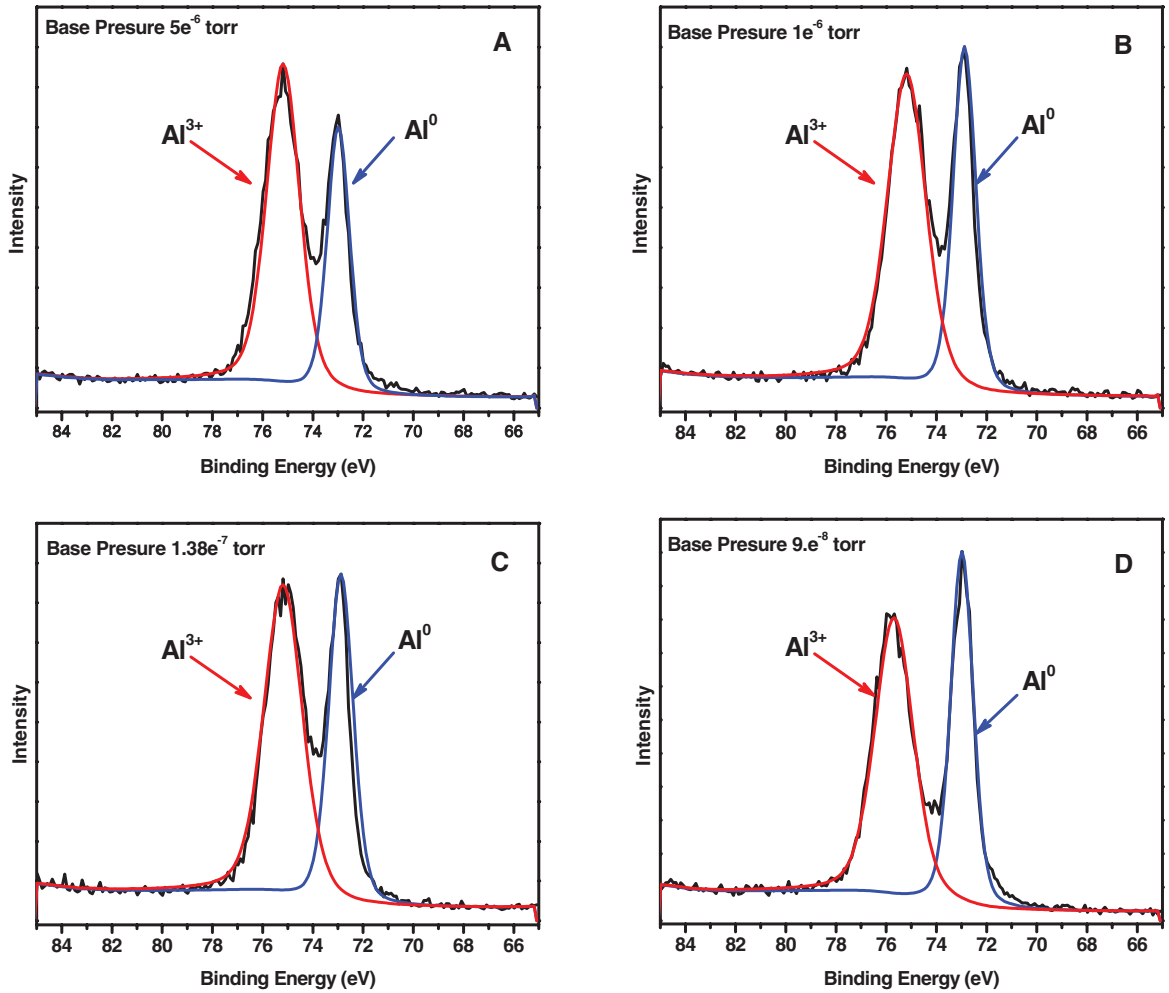

Figure 7. XPS high-resolution spectra of Al 2p for a) 5×10^{-6} torr, b) 1×10^{-6} torr, c) 1.38×10^{-7} torr and d) 9×10^{-8} torr.

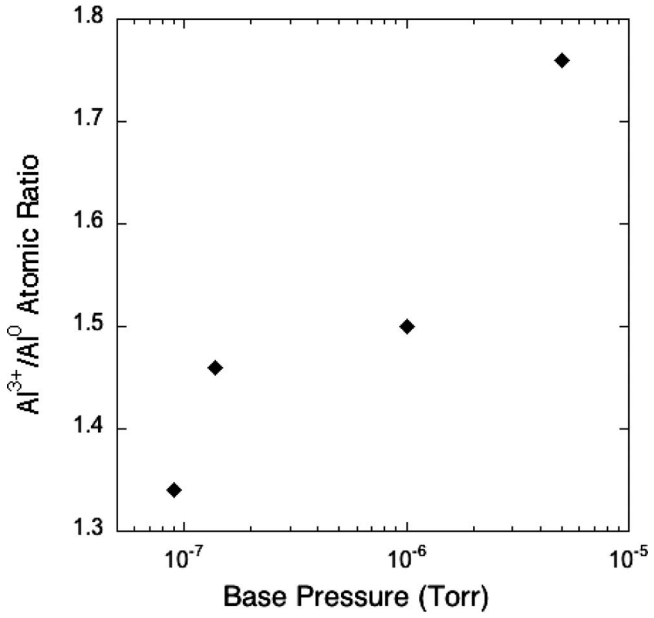

Figure 8. Al^{3+}/Al^{0} atomic ratio measured by XPS as a function of base pressure.

where I_o and I_m are the intensities (i.e. peak areas) of the metal and oxide photoelectron peaks, respectively. These data suggest that the surface oxide thickness increased monotonically, i.e. from 27.3 to 29.7 Å as the base pressure increased from 9.98×10^{-8} to 5.0×10^{-6} Torr. The Al target was also characterized by XPS following grinding to 2400 grit and cleaning with acetone. The oxide film on the target was thinner than that formed on any of the thin films, 26.3 Å. (It should be noted that sputtering of the target was performed for a period prior to deposition of the thin film to eliminate surface effects on the target.) It is possible that the initial oxidation of the freshly deposited samples was altered by the vacuum pressure or even that the oxidation began in the chamber before the chamber was vented to atmosphere.

TEM studies were performed, but not comprehensively pursued, in an attempt to assess the relative O:Al ratio using energy dispersive X-ray spectroscopy, EDXS, to corroborate the XPS findings. For the specimens studied, the grain size was in the vicinity of ∼100 nm for all the specimens observed (we observed all conditions excluding 5×10^{-6} torr). Only about 10 grains could be imaged per sample because there was significant fracture of the TEM grid windows as a result of the deposition. Regarding the grain size issue, as previously noted, it is not expected that any variation in the grain size could be responsible for the variation in E_{pit} of almost over the range of base pressures studied. The values of O:Al atomic concentration ratio determined from TEM-based EDXS are shown in Figure 9 as a function of base pressure. These results indicate that there is more O present in specimens with a higher base pressure (worse vacuum).

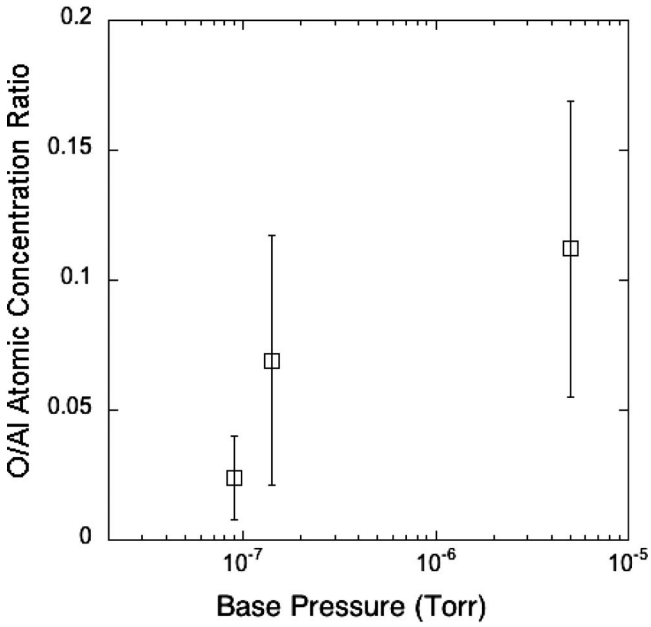

Figure 9. O/Al atomic ratio measured by DXDS as a function of base pressure.

Conclusions

The effect of sputter deposition system base pressure on the pitting corrosion resistance of pure Al thin films in NaCl solution was investigated. The following conclusions can be made:

1. The vacuum system base pressure had a significant effect on the corrosion resistance of sputtered aluminum, particularly evidenced by large variations in the pitting potential, E_{pit}. At the highest base pressure (worst vacuum), E_{pit} was almost 1 V higher than that of the bulk sample used as the target for the thin film deposition.
2. Pit growth studies revealed that E_{pit} and repassivation potentials were shifted in the noble direction with increasing base pressure. However, this shift in repassivation potentials was significantly smaller than that in E_{pit} and so cannot explain the very large increases in pitting potential.
3. Surface analysis by high resolution XPS spectra indicated a variation in the Al^{3+}/Al^{0} atomic ratio as a function of base pressure, perhaps as a result of the oxidation of the thin film sample in the deposition chamber.
4. Analytical TEM indicated that the O content in the deposit increased with base pressure, and changes in grain size were less significant.
5. To prevent oxygen uptake into the film, a maximum base pressure in the low 10^{-7} Torr range is recommended. The influence of oxygen, a chemical effect, is attributed as the key influence on the corrosion resistance of sputtered pure aluminum.

Acknowledgments

Financial support of the Australian Research Council is gratefully acknowledged. This work was performed in part at the Melbourne Centre for Nanofabrication (MCN) in the Victorian Node of the Australian National Fabrication Facility (ANFF).

References

1. R. B. Inturi and Z. Szklarska-Smialowska, *Corrosion*, **48**, 398 (1992).
2. R. B. Inturi and Z. Szklarska-Smialowska, *Corrosion Science*, **34**, 1973 (1993).
3. R. B. Inturi and Z. Szklarska-Smialowska, *Corrosion Science*, **34**, 1201 (1993).
4. L. Liu, Y. Li, and F. H. Wang, *Electrochimica Acta*, **52**, 7193 (2007).
5. L. Liu, Y. Li, and F. H. Wang, *Electrochimica Acta*, **52**, 2392 (2007).
6. L. Liu, Y. Li, and F. H. Wang, *Electrochimica Acta*, **53**, 2453 (2008).
7. C. Pan, L. Liu, Y. Li, and F. H. Wang, *Thin Solid Films*, **519**, 4781 (2011).
8. S. I. Pyun, E. J. Lee, and G. S. Han, *Thin Solid Films*, **239**, 74 (1994).
9. M. P. Ryan, N. J. Laycock, R. C. Newman, and H. S. Isaacs, *Journal of the Electrochemical Society*, **145**, 1566 (1998).
10. B. Zhang, Y. Li, and F. H. Wang, *Corrosion Science*, **49**, 2071 (2007).
11. Y. P. Zhao, C. F. Cheng, G. C. Wang, and T. M. Lu, *Applied Physics Letters*, **73**, 2432 (1998).
12. G. S. Frankel, *Corrosion Science*, **30**, 1203 (1990).
13. W. C. Moshier, G. D. Davis, J. S. Ahearn, and H. F. Hough, *Journal of the Electrochemical Society*, **134**, 2677 (1987).
14. K. D. Ralston and N. Birbilis, *Corrosion*, **66**, 075005 (2010).
15. K. D. Ralston, N. Birbilis, and C. H. J. Davies, *Scripta Materialia*, **63**, 1201 (2010).
16. K. D. Ralston, D. Fabijanic, and N. Birbilis, *Electrochimica Acta*, **56**, 1729 (2011).
17. R. B. Inturi and Z. Szklarska-Smialowska, *Corrosion Science*, **34**, 705 (1993).
18. G. S. Frankel, R. C. Newman, C. V. Jahnes, and M. A. Russak, *Journal of the Electrochemical Society*, **140**, 2192 (1993).
19. G. S. Frankel, *Electrochemical Methods in Corrosion: Research and Application*, Transtec Publications Ltd., Zurich, Switzerland (1997).
20. G. Z. Meng, L. Y. Wei, T. Zhang, Y. W. Shao, F. H. Wang, C. F. Dong, and X. G. Li, *Corrosion Science*, **51**, 2151 (2009).
21. S. J. Orr, S. I. Pyun, and S. W. Nam, *Thin Solid Films*, **279**, 7 (1996).
22. J. Borges, C. Fonseca, N. P. Barradas, E. Alves, T. Girardeau, F. Paumier, F. Vaz, and L. Marques, *Electrochim. Acta*, (2013).
23. F. Aviles, O. Ceh, and A. I. Oliva, *Surface Review and Letters*, **12**, 101 (2005).
24. G. S. Frankel, J. O. Dukovic, V. Brusic, B. M. Rush, and C. V. Jahnes, *Journal of the Electrochemical Society*, **139**, 2196 (1992).
25. A. Kolics, A. S. Besing, P. Baradlai, R. Haasch, and A. Wieckowski, *Journal of the Electrochemical Society*, **148**, B251 (2001).
26. B. R. Strohmeier, *Journal of Vacuum Science & Technology a-Vacuum Surfaces and Films*, **8**, 3347 (1990).